A screened Coulomb scattering module for displacement damage computations in Geant4

Robert A. Weller, Senior Member, IEEE, Marcus H. Mendenhall and Daniel M. Fleetwood, Fellow, IEEE

Abstract

A new software module adding screened Coulomb scattering to the Monte Carlo radiation simulation code Geant4 has been applied to compute the nonionizing component of energy deposited in semiconductor materials by energetic protons and other forms of radiation. This method makes it possible to create three-dimensional maps of nonionizing energy deposition from all radiation sources in structures with complex compositions and geometries. Essential aspects of previous NIEL computations are confirmed, and issues are addressed both about the generality of NIEL and the ability of beam experiments to simulate the space environment with high fidelity, particularly for light ion irradiation at very high energy. A comparison of the displacement energy deposited by electromagnetic and hadronic interactions of a proton beam with published data on GaAs LED degradation supports the conclusion of previous authors that swift light ions and slower heavy ions produce electrically active defects with differing efficiencies. These results emphasize that, for devices with extremely small dimensions, it is increasingly difficult to predict the response of components in space without the assistance of computational modeling.

I Introduction

Displacement damage can lead to degradation of performance and ultimately device failure in many kinds of semiconductor devices [1]. These concerns are particularly acute for devices that must operate in space, where radiation is plentiful and spare parts are few [2]. This paper describes a new approach to computing the portion of energy that radiation deposits in a device in the form of atomic motion. It would, of course, be preferable to directly compute the distribution of electrically active defects. However, what constitutes a defect in the electrical sense is surprisingly ambiguous, and may also change over time through annealing. Thus, the energy deposited in atomic motion is taken here and elsewhere as a measure of initial displacement damage.

Research Supported in part by NASA, DTRA, and the DOD MFEL program under grant FA9550-04-1-0045.

Corresponding author Robert Weller is with the Vanderbilt University Department of Electrical Engineering and Computer Science and the Institute for Space and Defense Electronics (ISDE). email:robert.a.weller@vanderbilt.edu, phone (615)343-6027.

Daniel Fleetwood is with the Vanderbilt University Department of Electrical Engineering and Computer Science.

Marcus Mendenhall is with the Vanderbilt University W. M. Keck Free Electron Laser Center and the Department of Physics and Astronomy.

The most common measure of displacement damage in the literature has been nonionizing energy loss (NIEL) [3] [4]. However, the application of NIEL to predict device response is not always straightforward, as has been recognized in the literature [1], and as we discuss further below. In this paper we describe a new approach to computing damage energy made possible by an extension of the Geant4 Monte Carlo radiation simulation system [5] that models screened Coulomb collisions between nuclei [6]. Because Geant4 already includes sophisticated nuclear-reaction physics and the ability to track particles through complex geometrical structures, modeling essentially all of their physical interactions and those of arbitrarily numerous generations of daughter particles, the new Coulomb scattering addition makes it possible, for example, to directly address the observed discrepancy at high energies between NIEL and measured damage in GaAs LEDs [7][8] in a fundamentally different way. We have found that the new computation predicts the scaling of the data with incident particle energy, but with an important caveat: the efficiency of producing electrically active defects is not a function of the quantity of deposited collisional energy alone [7]. This has been observed before, and attempts have been made to modify the computation of NIEL to account for it [9][10]. However, our interpretation is fundamentally different.

The discrepancy between the conventional NIEL and published GaAs LED data strongly suggests that the concept of a single energy-based measure of electrically active damage has reached its limits of validity, and that microscopic, device-dependent modeling of displacement damage, combining both more sophisticated energy deposition computations and theoretical modeling of the electrical properties of disordered regions, is required to predict with higher confidence the response of sensitive devices to displacement damage in space. The procedure described here generates physically realistic distributions of deposited energy in three-dimensional micro-volumes, tracing particles cascades down to the limits imposed by the binary collision approximation, and so forms the basis upon which such a comprehensive strategy may be built.

II Simulation Methodology

The details of the module that we have added to Geant4 are described in a separate paper [6]. The statistical techniques are similar to those that relate scattering angle to impact parameter in the well-known TRIM [11] and SRIM [12] codes. These are supplemented by a more sophisticated inter-atomic-collision cross section using an extension of an algorithm that is described in [13]. The interaction potential between colliding atoms may be selected from a predefined set or may be specified by the user. In the case of the curves published here, we have used the universal screening function of Ziegler, Biersack and Littmark [14]. However, we do not use the same method to obtain a cross section, or more precisely a randomized scattering angle. TRIM and SRIM use an approximation called the magic formula that is a large-angle extrapolation of an exact small-angle result [15]. This approach has recently been applied to estimate NIEL [16] in a formalism that follows quite closely the well established stopping theory of Lindhard, Scharff and Schiøtt [17] with additions by later authors.

By contrast, we use a modification of the algorithm described in [13] that computes an exact scattering angle as a function of impact parameter for events below projectile energies of approximately 100 MeV per nucleon, and in the relativistic region above this, returns an approximation in good agreement with, *e.g.*, the expression of Seitz and Koehler [18] used by

Burke [3]. Although less sophisticated than the recent state of the art in relativistic collisions [19], it is completely satisfactory for the present purposes. As described in [6], the screened scattering process supplements existing Geant4 nuclear reaction processes, such as the binary cascade model of nuclear reactions that was used for in this work. Similarly, Geant4 elastic hadronic scattering was also used as described in [6].

The approach described here differs from previous Monte Carlo computations [20] in explicitly tracking all particles, including electrons, photons and neutrons from both electromagnetic and hadronic interactions, along with daughter particles of all orders, until all have either come to rest or left the experimental volume. The energy deposited in the host material by all processes, whether ionizing or nonionizing, can be tracked as a function of position and time, and distinguished by interaction type.

The contributions to nonionizing energy density from primary knock-on atoms (PKAs) and daughters of nuclear reaction fragments, although conceptually identical for many purposes, were recorded separately. These quantities were computed by tracking the kinetic energy of PKAs and nuclear reaction fragments, and all secondary particles created by these primaries. Each particle was followed from its creation until its kinetic energy fell below 1 keV. As it traveled, its discrete interactions with the lattice atoms down to an energy transfer of 1 eV were recorded. Any interaction that transferred less than 1 keV of energy (the large majority of interactions) resulted in the tabulated energy at that point in space being increased, and the ion energy decreased correspondingly. If a collision resulted in the transfer of more than 1 keV, a daughter particle was created and tracked. When a moving ion finally fell below the 1 keV threshold, it was stopped in place, and its kinetic energy added to the accumulated nonionizing energy at that point. A three dimensional map of deposited energy density $F(\vec{z},\vec{p};\vec{x})$ at $\vec{x}$, as a function of initial location $\vec{z}$ and momentum $\vec{p}$ of the primary ion was produced in this way. The nonionizing energy deposition rate (NIEDR), a quantity that approximates NIEL, was computed from $F(\vec{z},\vec{p};\vec{x})$ as described in Appendix A.

The 1 keV threshold was arbitrary and user-selectable. However, tracking to energies much below approximately 1 keV fundamentally violates the assumptions of a binary collision model, and should be carried out separately by a full molecular dynamics code, if such detail is desired. If ion-channeling effects are also of concern, then the threshold to transition to molecular dynamics should probably be even higher. The number of events sampled for each data point ranged from tens of thousands to hundreds of millions depending on the situation and the quantity desired.

The basic physics of the screened collisions in matter was verified by comparison with three classes of scattering measurements, Rutherford backscattering, ion implantation and small angle multiple scattering of ions passing through foils [6]. The Rutherford backscattering cross section is known theoretically. To test direct and inverse kinematics, the ion implantation ranges and range straggling were compared for boron and arsenic implanted into Si using as a standard the SRIM program, which has been extensively compared with experiment. The screened Coulomb scattering process automatically implements the concept of multiple scattering through repeated small angle collisions, and unlike the default Geant4 multiple scattering process, it spawns secondary particles that are themselves tracked [6]. There is a wealth of data on multiple

scattering in the literature of nuclear and particle-solid interaction physics, and the shapes of the angular distributions for various foil thicknesses are well known [21]. The present computation predicts the angular distribution of protons and alpha particles in carbon foils with high accuracy. In fact, when the screened Coulomb scattering process is being used, multiple scattering as a separate process in Geant4 is redundant and should be disabled for nuclei.

III Results

Fig. 1 shows the result of a computation of nonionizing energy deposition rate (NIEDR) in GaAs along with the data of Barry *et al.* [7]. Also shown is the NIEL curve of Burke *et al.* [4][10], which has been digitized from Fig. 3 of [7], and a NIEL curve from [22] obtained by applying Bragg's rule to tabulated numerical values of Ga and As NIEL. The NIEDR attributable to direct interactions of the proton beam and target nuclei and that by heavy hadronic elastic recoils and residual nuclei are displayed separately. The similarity between the curve giving the beam-generated displacement energy (the solid dots, denoting the relativistic Coulombic calculation) and the data of [7] is striking, and suggests that Coulombic elastic interactions of the beam generate electrically active defects more efficiently on a per-unit-energy basis than do the residual nuclei [9].

Fig. 2 shows the NIEDR curves as in Fig. 1 computed for protons in Si, along with the NIEL value for protons in Si from [22]. Again the contributions to NIEDR from direct beam-target interactions and those from residual recoil nuclei are shown separately. The numerical differences, particularly at high energies, underscore that NIEDR and NIEL, while similar in concept, are potentially different in detail.

To gather insight into the microstructural differences between direct beam effects and those by residual nuclei, we have examined the makeup and energy of nuclear reaction fragments as well as the three dimensional microstructure of a number of discrete nuclear reaction events occurring in GaAs and Si. A stereogram of such an event in GaAs is presented in Fig. 3.

In Fig. 3 the ionizing (black) and nonionizing (red) energy density are shown as a function of position for a single 100 MeV proton (green trajectory) interacting with ^{75}As in GaAs. Energy density information is superposed with particle trajectory information for neutrons to form a complete image of the event. Two views of the event with different length scales are presented, with Fig. 3(b) showing greater detail around the nuclear reaction vertex. Fig. 3(b) is also rotated by a few degrees relative to Fig. 3(a). Three widely dispersed regions with displacement damage indicated by red dots (with red circles around them so they can be found) produced by the recoiling spallation products are visible in the upper figure.

The heavy residual nucleus, which moves downward from the vertex, produces extensive and concentrated displacement damage. Neutrons from the nuclear reaction, which don't interact otherwise, are shown as cyan trajectories. Gamma rays are not shown. This figure illustrates graphically the qualitative difference in displacement damage produced by swift light ions and slower heavy ions. By fusing these images visually, the three-dimensional structure of the reaction can be observed.

IV Discussion

The data of Barry, *et al.* [7] shown in Fig. 1 have engendered a substantial discussion in the literature. (See reference [1] and references therein.) The issue can be stated succinctly. When applied to silicon systems, NIEL as defined below, has been successful in predicting electrical

effects attributed to displacement damage. However, when the same methodology was applied to the GaAs system, the disagreement shown in Fig. 1 resulted. Specifically, for silicon systems it appears to be appropriate to simply add the contributions from direct beam-target interactions and from recoil nuclei created in nuclear reactions to obtain an overall NIEL. One concludes from the data of Barry, *et al.* [7] that same methodology does not work for GaAs. The question was, and is, why, and more importantly, in light of this finding, how can one be confident that NIEL can be used as an *a priori* predictor of electrical displacement damage effects? In consideration of this question, let us look closely at the definition of NIEL.

Physically, NIEL is a variation of nuclear stopping power that includes a correction designed to exclude energy expended in ionization by recoil particles. Unlike nuclear stopping power, it also explicitly includes nuclear reactions in addition to elastic ion-atom collisions. Burke first articulated the concept of NIEL as it is presently employed [3][4][10], and Jun has recently introduced an important modification to the procedure for calculating it [23]. Additional changes have been proposed by Messenger *et al.* in [9] with yet more refinements in [16]. Akkerman *et al.* use another relatively distinct approach [24]. References [4][16][23][24] have the clearest mathematical statements of the definition, and the method of [23] has been widely adopted (*e.g.* [16][22][25]). The comments that follow apply most directly to the original procedure described by Burke [3][4][10], but they are generally applicable.

NIEL is a measure of that portion of energy lost by a quantum of radiation, per unit of trajectory, at a specific point, that ultimately ends up somewhere in a (hypothetically infinite) target in the form of whole-atom motion. Thus, while its numerical value is assigned at a point, the value measures effects that are non-local [10]. NIEL is ordinarily defined by the following expression, which is a composite of equations from [4] and [23]:

$$NIEL(E) = \frac{N_A}{A} \sum_i L(T)\, T \cdot d\sigma_i(E,T) \tag{1}$$

Here $d\sigma_i(E,T)$ is the differential cross section for a particle with energy E to create a secondary particle with kinetic energy T, $L(T)$ is a quantity called the Lindhard partition function [26], N_A is Avogadro's number, A is the molar atomic mass in g/cm^3, and the summation and integration are assumed to be over all kinematically-permitted processes. Both [4] and [23] distinguish Coulomb scattering and nuclear reaction events as distinct elements of the sum. Reference [4] applies the Lindhard partition to the average energy of nuclear recoils, while [23] uses MCNPX, another Monte Carlo radiation code [27], to obtain information on nuclear reaction fragments.

To understand (1), consider a simple modification of the Coulomb term involving the total cross section for Coulomb collisions. This Coulomb scattering term appears in both [4] and [23].

$$\left|\frac{dE}{dx}\right| dx = N(\sigma_{total} dx) \int (L(T) \to 1) \cdot T \frac{d\sigma_C}{\sigma_{total}} \tag{2}$$

Here N is the density of target atoms in cm^{-3}, ρ is the target density in g/cm^3, and we have introduced a differential energy loss $|dE/dx|$ as the particle moves a distance dx at position x. The term $d\sigma_C/\sigma_{total}$ is just the probability of transferring energy T in a collision. Setting $L(T)=1$ for a moment, the integral is then the average energy $\langle T \rangle$ transferred in a collision. The term $\sigma_{total} dx$ is a volume. If σ_{total} is interpreted as the transverse area of the projectile, then $\sigma_{total} dx$ is the volume that the projectile sweeps out in moving a distance dx, the volume in which all target atoms will

be hit. To obtain the number of particles in this volume, one multiplies by N. To obtain the average energy lost by the projectile in all collisions in this volume, one also multiplies by $\langle T \rangle$. The result is:

$$\left|\frac{dE}{dx}\right| = N\sigma_{total}\int T\frac{d\sigma_C}{\sigma_{total}} = N\int T\cdot d\sigma_C \tag{3}$$

This is the well-known expression for linear energy transfer (LET), or stopping power [28]. All that remains is to divide by the density ρ of the target to obtain the usual unit. The critical point to be recognized is that LET refers to the beam and not to the target. It specifies how much energy the beam loses for a given increment of trajectory. It does not say how much energy is deposited locally at a point in the target. Of course, through conservation of energy, the energy lost by the beam must end up somewhere, but LET does not specify where. Instead, ion track models must be invoked to describe how the ion's energy is distributed [29].

NIEL blurs the distinction between a beam and a device property. Its value quantifies the energy surrendered by the beam at a given point, without regard to where that energy ultimately manifests itself in a device. For practical applications, it is the disorder in the three dimensional sensitive volume of a device, and more specifically the disorder that leads to electrically active defects, that is important. NIEL does not attempt to do this spatial bookkeeping.

In the mathematical notation usually used when NIEL is defined, this non-local aspect of the value is not obvious. This ambiguity in NIEL has been recognized and in [10] the authors considered the effects of particle equilibrium near a surface and defined "restricted energy loss" to compensate, but to date no other method of describing (the potential for) displacement damage on a scale comparable to modern logic devices has been proposed. Similar arguments apply to LET, of course, but for predicting the details of charge deposition, LET is augmented with a radial track model. The situation with displacement damage is more complicated because, as a structural modification in the semiconductor material, it is relatively permanent and it has electrical properties that depend on the extent and atomic-scale structure of the damaged region.

The spatial uncertainty is further complicated by $L(T)$, the Lindhard partition function [26][30]. $L(T)$ is the fraction of the energy T of a primary recoil that is not consumed in electron-hole pair creation. Thus, its inclusion in (1) would appear to be straightforward and well justified. However, the integral equation from which $L(T)$ is derived is a function only of the energy of the primary particle and assumes implicitly an infinite, homogeneous, isotropic medium for the full development of a cascade event. Consequently, equation (1) causes all of the energy of a secondary particle to be accounted for at the location of its creation, even if that energy is actually deposited many microns away. For this reason, low mass nuclear fragments are normally excluded from NIEL computations using (1). However, even relatively frequently occurring residual nuclei from, e.g., cosmic ray proton bombardment, have ranges of several microns.

When one is calculating ionizing radiation effects of protons (*e.g.*, single event effects) using LET, the intrinsic variability of secondary electron ranges along a particle track does not lead to significant difficulties in the results, except in structures with dimensions on the order of the track diameter. However, protons and other particles with energy in the electronic stopping regime deposit their collisional (non-ionizing) energy *preferentially at the ends of their ranges*. In the approach discussed here, the requisite physics is included within the computation, so that

it is not necessary to invoke $L(T)$. Since the deposited energy is recorded as a function of position in the three-dimensional device structure, the non-locality problem does not arise. In fact, the present method can be used to compute $L(T)$. Appendix B contains additional information on $L(T)$ including a figure showing its computed values for Si recoils and protons in silicon for several target thicknesses.

In beam experiments the maximum energy of recoil particles is ordinarily in the velocity-proportional stopping region, on the low-energy side of the Bragg peak of the LET curve. Such particles have the greatest rate of energy loss when they are created, and they tend to deposit their energy in the vicinity of their point of origin, much as the ionization generated by LET. Moreover, at low energies, the directionality of atomic collisions in solids becomes less extreme. Thus, when recoils are low in energy, as shown in Fig. 1, NIEL gives a credible result, in spite of any possible conceptual subtleties with its definition.

When the requisite conditions identified for NIEL validity are in question, specifically when primary particles are swift, nuclear reactions occur, or device dimensions are small compared with the range of secondary particles, caution in relating NIEL values to displacement damage at specific locations is appropriate [9][10].

The nonionizing energy density defined in Appendix A conveys much more spatial information than NIEL. Thus, one might reasonably ask whether or not the discrepancy between the computation and data shown in Fig. 1 could have been anticipated in advance and whether future discrepancies will now be anticipated. It is not the purpose of this paper to answer this question, but rather to introduce a technique that may in the future be instrumental in doing so. Nevertheless, in light of the *observed* discrepancy, it is possible to recognize warning signs which in retrospect might have raised questions about the *relative* appropriateness of simply adding NIEL for protons and recoil nuclei in the Si and GaAs systems.

In analyzing the fragmentation patters of nuclei in Si and GaAs using Geant4, two things become apparent. First and obviously, the recoil nuclei are higher in mass for the GaAs system. Less obviously, the recoil nuclei from the Si breakup are higher in energy. Roughly, this happens for two reasons. First, the asymmetry between the spallation and recoil fragments is lower for Si so that momentum sharing implies more energy for the heavy fragment. Second, the Si reaction appears to emit alpha particles more frequently. These result in much more momentum and energy being transmitted to the fragment. In addition, smaller fragments, e.g. O are much more frequent than in the GaAs system.

It is well known in the study of atomic collisions in solids that slow heavy ions in high-atomic-mass targets produce dense and closely spaced collision cascades. From a comparison of the mass and energy distributions of the residual recoil nuclei from reactions in Si and GaAs, one may conclude that the damage in GaAs (Fig. 3) should be significantly more concentrated. Also, the correlation length of conduction electrons, as measured by the Bohr radius of neutral donor impurities, is larger by a factor of approximately 4 in GaAs than in Si. Together, these observations suggest that displacement damage from residual nuclei in Si may appear to conduction electrons more like random beam-generated collision cascades than does similar damage in GaAs.

A final point worth keeping in mind concerns statistics. Assuming a geometrical cross section of roughly 0.4 to 0.8 barns for Si, Ga and As, the probability of one event like that of Fig. 3 in a given cubic μm of material for a $10^{11} cm^{-2}$ fluence of protons is only about 0.2-0.3%. (In [7] the highest reported fluence is about $6 \times 10^{10} cm^{-2}$.) It is entirely possible in some circumstances that

averaging the recoil nucleus contribution to energy deposition may be inappropriate by virtue of the expected total number of such events. By this observation, we do not intend to assert that this is the explanation for the experiment discussed in [7]. We simply observe that if one computes the average NIEL or deposited energy density with a numerically convenient virtual flux, it may or may not represent the expectation in an experiment where counting statistics of small numbers becomes important. In such a limit, it will be necessary to explore computationally the response of individual devices to ensembles of random events such as shown in Fig. 3 to assess device effects. This will, in turn, require advances in the theory that relates deposited energy to the type, density, and arrangement of electrically active defects.

V. Simulation Fidelity in Beam Experiments

An indirect but potentially very important benefit of the Monte Carlo approach to displacement estimation is the ability to handle complex radiation environments without the need to separately propagate them to the sensitive region of a device. Understanding this issue is crucial to judging the ability of beam experiments to evaluate accurately the sensitivities of devices to displacement damage in space. A particular challenge, as also recognized in previous studies (*e.g.*, [7][31]) is establishing secondary particle equilibrium in beam experiments. In space, radiation is omni directional and distributed in energy. In a beam experiment, particles typically are unidirectional and approximately monoenergetic. Length scales are dramatically different to establish secondary particle equilibrium for ionization effects and displacement effects, owing to the very different ranges of the secondary particles that ultimately lead to electrically active defects in these interactions. Moreover, length scales to establish particle equilibrium are much smaller (approximately a few μm) for slow heavy ions as opposed to the vastly longer length scales of swift light ions ($>>1 mm$ for high-energy proton beams) [10].

For devices of most interest to modern microelectronics and photonics in space, device dimensions of interest increasingly are less than $1 \mu m$, and in many significant device types are at or approaching nanoscale dimensions. This means that the interactions that cause detectable damage in a particular device region increasingly are caused by events that are initiated outside the electrically sensitive region.

In beam experiments, scattering events tend to be biased towards the forward direction. Unless the surrounding layers are sufficiently thick to ensure that "scatter in" events causing damage in beam experiments balance the particles that scatter out of the sensitive region, device degradation in space (where surrounding materials typically ensure particle equilibrium) likely will be underestimated. Summers et al. have introduced "restricted energy loss" [10] specifically to account for such effects. Using the methods described here, such assumptions are unnecessary. Calculations that correctly include all relevant interactions with the device and its surroundings are possible, so that even non-equilibrium situations are handled correctly.

These considerations are also important for single event effects. A particularly dramatic example of the kinds of effects one may see owing in part to issues of secondary particle equilibrium is the strong angular dependence of photocurrent in modern electronic circuits [32][33] and optocouplers [34]. A simple calculation of particle ranges in the semiconductor of interest [34] shows that, at moderate proton energies (10-60 MeV), one easily moves from a condition in which one is well outside of secondary electronic equilibrium for normal incidence beam irradiation into a case where one establishes particle equilibrium when the beam must pass through intervening packaging and surrounding device layers. This adds to the other geometrical

and beam physics effects discussed explicitly in Refs. [32][33][34], and can induce extreme variability in device response for cases in which small changes in angular positioning introduce a significant change in the amount of forward-scattering material through which the beam must pass. For higher energy proton irradiation (*e.g.*, ~200 MeV), the device is not within particle equilibrium at *any* typical beam experiment configuration, leading to an elimination of the angular effect, as observed experimentally [33]. While these examples are for ionization damage, similar effects must occur in displacement damage experiments. When the active volume of the device includes stopped particles, defect densities will exceed those measured when it does not. With the assistance of Geant4 computations, one can improve the design and interpretation of these kinds of experiments. Without sophisticated computational assistance, extrapolating from beam experiments to space response becomes increasingly difficult for modern space electronics and photonics technologies [10]. The new computational methods discussed here should help to improve the simulation fidelity of beam experiments significantly.

VI. Conclusions

A screened Coulomb scattering module has been developed for Geant4. Relevant scattering characteristics have been verified by comparison with Rutherford scattering, ion implantation, and small-angle multiple scattering analytic computations and data. The resulting Geant4-based tool is directly applicable for computing three-dimensional maps of nonionizing energy density in semiconductor devices with arbitrary materials and geometries. This includes contributions from primary and secondary ions of all orders, as well as those from hadronic reactions and even elementary particles. An application of this tool to GaAs has reproduced the variation of damage coefficient in GaAs light-emitting diodes from proton radiation over several orders of magnitude in proton energy. However, it has been necessary to distinguish between damage produced by light ions and heavy recoils, and to assume that the latter generate *electrically active* defects less efficiently on a per-unit-energy basis [7].

The concept of NIEL has been examined critically and potential limitations involving the location of deposited energy and the use of the Lindhard partition function have been identified. Although minimized by recent improvements in the strategy for computing NIEL, these issues serve to underscore the ultimate difficulty of characterizing radiation-induced displacement damage in a semiconductor device with a single energy-derived parameter. A more general measure of initial average displacement damage, the nonionizing (or displacement) energy density, has been defined (Appendix B), and an expression has been given that relates it to the average energy deposition rate along path by the primary ion. Computed by Monte Carlo techniques, nonionizing energy density averages the effect of the radiation flux in a specific device, yielding a measure of damage that is a function of position, and dependent upon not only the local materials properties, but also those of the immediate environment.

Unfortunately, no average can capture extreme single event behavior. For this reason, in the absence of a theory relating nonionizing energy deposition to electrically active defects, it is advisable to distinguish the nonionizing contributions from Coulomb scattering and hadronic reactions in a computation, and to consider them separately when comparing computed damage energy with experiments. Similarly, it may be useful to distinguish displacement events from events that generate phonons (collisions transferring an amount of energy below the displacement threshold). The methods proposed here make it possible to do all these things, and as such establish a basis for quantitative studies of the relationship between microscopic structure of energy deposition and the production of electrically active defects. When fully

implemented, these techniques will significantly improve predictions of space response from beam experiments.

Appendix A

The availability of screened Coulomb scattering in Geant4 leads naturally to the definition of a new energy deposition parameter that complements and extends NIEL. This parameter is $F(\vec{z},\vec{p};\vec{x})$, the average nonionizing energy deposited per unit volume at location $\vec{x}$ by a source particle with momentum $\vec{p}$ initially located at position $\vec{z}$. $F(\vec{z},\vec{p};\vec{x})$ is a field defined at all points within and around the target, which embodies the intent of NIEL without sacrificing the spatial information that is lost by using $L(T)$ and referring energy back to the ion loss rate. The nonionizing energy deposition rate (NIEDR), which has the same units as NIEL and which approximates it in value, can be derived from $F(\vec{z},\vec{p};\vec{x})$. NIEDR describes the nonionizing energy deposited per unit length of particle trajectory in the initial direction, at a specific range z and is defined as follows:

$$NIEL(E(p,z)) \simeq NIEDR(p,z) = \iint F(\vec{0}, p\hat{k}, z\hat{k})dx\,dy \tag{4}$$

Here the particle's initial point is assumed to at the origin of the coordinate system, with initial momentum $p\hat{k}$ in the $+z$ direction, as indicated by the unit vector $\hat{k}$. $E(p,z)$ is the energy of the particle at location z given initial momentum p at location $\vec{0}$. The double integral is over the plane transverse to the particle's direction of travel. So defined, NIEDR has the expected unit of energy/length (where length is often expressed in g/cm^2 of target material by dividing by the density ρ) and is a function of the projectile's initial momentum and the point of observation $\vec{x} = z\hat{k}$. (The deposition rate is also a function of energy through the range-energy relationship $E(p,z)$.) NIEL, on the other hand, is naturally a function of particle velocity and is thus usually expressed directly as a function of energy. The curves in Figs. 1 and 2 of this publication were obtained from the Geant4 simulation of protons in GaAs and Si respectively by reducing $F(\vec{z},\vec{p};\vec{x})$ to NIEDR, for direct comparison with NIEL and the data. For numerical convenience, the average NIEDR over a 10 μm thickness in z was computed, but no other corrections were make to the value as defined in equation (4). Fig. 3, on the other hand, is a visualization of $F(\vec{z},\vec{p};\vec{x})$ with particle trajectories superimposed to provide context.

The use of a distribution function such as $F(\vec{z},\vec{p};\vec{x})$ to describe atomic collisions in solids is not a new idea. Winterbon, Sigmund and Sanders [35] presented an integral equation for $F(\vec{z},\vec{p};\vec{x})$ in a homogeneous, isotropic, elemental material, and solved it for restricted collision cross sections and low-energy primary particles. However, the complexity of a real semiconductor device, heterogeneous in composition and intricate in geometry, is so great by comparison that it does not make sense to even write down the generalized transport equations, much less attempt to solve them. The only practical approach to the solution is Monte Carlo simulation. The approach presented in this paper is quite literally a Monte Carlo solution of a transport equation for the quantity $F(\vec{z},\vec{p};\vec{x})$. However, even this added level of complexity cannot be assumed to

be sufficient, since $F(\vec{z},\vec{p};\vec{x})$ is itself composed of components (*e.g.* phonon energy density and displacement energy density), and like NIEL *it is an average*.

In order to understand the significance of $F(\vec{z},\vec{p};\vec{x})$ being an average, it is necessary to visualize a specific event. The average $F(\vec{z},\vec{p};\vec{x})$ is related to the energy deposition of the i^{th} particle in a Monte Carlo simulation through:

$$F(\vec{z},\vec{p};\vec{x}) = \frac{1}{N}\sum_{n=1}^{N} F_n(\vec{z},\vec{p};\vec{x}) \tag{5}$$

Here $F_n(\vec{z},\vec{p};\vec{x})$ is the nonionizing energy density at $\vec{x}$ produced by a single incident ion. It is a particular strength of the present approach that physically based statistical information on extreme displacement events is contained in the distribution of the $F_n(\vec{z},\vec{p};\vec{x})$. In the region where NIEL has difficulties (*e.g.*, well above 10 MeV in Fig. 1), there are two classes of events with significantly different properties. Events that deposit lattice energy through the direct generation of primary recoils are by far the most numerous, and their contribution is sufficient alone to account for the trend of the data presented in Fig. 1. Events such as that shown in Fig. 3 that involve a nuclear reaction are of a substantially different character.

Fig. 3 is a stereogram of the vertex region of a nuclear reaction, shown at two different length scales. It is actually a composite diagram showing both energy density in red (typically red dots corresponding roughly to 2 nm voxels), and for context particle trajectories as well. A 100 MeV proton (green trajectory) enters from the right and strikes an ^{75}As nucleus producing numerous fragments. Neutrons are shown as cyan trajectories and produce no secondary displacement or ionization. Gamma rays are omitted from the figure. The low-mass charged fragment trajectories may be identified as the origin of numerous delta electron tracks, shown as thin gray lines. Barely visible along the particle trajectories are several red dots (with red circles to aid location), indicating the locations of regions of displacement energy deposition. Although these are often referred to as point defects, their actual structure is likely to be more complex.

The short chain of red dots, shown in enlarged form in the lower Fig. 3(b), is a series of discrete displacement damage regions produced by the ^{62}Ni recoil nucleus, which has an energy of ~2.9 MeV. The distance from the vertex to the final location of this recoil is about $0.5\,\mu m$. This compares with a mean range for 3 MeV ^{62}Ni in GaAs of about $1.2\,\mu m$, as computed with Geant4 using the screened Coulomb scattering module described above. The displacement energy deposited by the ^{62}Ni fragment is ~200 keV.

Most of the red dots, which are derived from energy deposition data recorded on a 1 nm grid, represent a single stopped recoil with energy $<1\,keV$. A few have substructure. Generally, this means that the disordered regions are at most a few nm in diameter and probably only about 2-4 nm in diameter. Note finally at the top of Fig. 3(b) that one of the displacement events produced by a charged spallation fragment is visible. Although spallation nuclear reactions, which dominate for high-energy protons, often result in several very energetic low-mass charged fragments, the total nonionizing energy that these fragments deposit in the sensitive volume (specifically for the case shown in Fig. 1 and the event of Fig. 3) is usually trivial compared with the energy of the heavy recoiling residual nucleus or of the recoil nucleus in a hadronic elastic scattering event [4].

Coulomb interactions by highly energetic light nuclei produce occasional and widely dispersed damage regions and are relatively frequent. Reaction fragments and high-energy, heavy elastic recoils produce massive, correlated damage of the kind shown in Fig. 3 and are very infrequent. There is no reason a priori to believe that the yields of *electrically active* defects from these two events are commensurate [1][10][24][36]. In fact, the data of Fig. 1 argue strongly that they are not.

In Fig. 1, the energy density attributable to heavy recoils is shown separately, but in the correct ratio to the elastic recoil contribution. The success of the Coulomb curve in alone capturing the trend in the data suggests that electrically active defects produced by heavy recoils come at a higher price energetically [1][10][24][36]. Indeed the clusters in Fig. 3, although small, may contain hundreds of displaced atoms. Thus, relatively large regions of disorder may be acting collectively from an electrical perspective [1][7][37].

One measure of the correlation length of an electron in GaAs, the Bohr radius of a neutral donor impurity is ~10 nm. This is large enough to encompass an entire damage cascade and perhaps multiple cascades. In Si on the other hand, this value is about four times smaller. Along with the energetics of the recoils and the resulting collision cascade densities, these observations lead us to a conservative hypothesis that the displacement energy from Coulomb scattering by the beam and by residual nuclei from nuclear reactions should not be combined unless it can be shown that the electrical characteristics of the resulting damage warrant such an approximation. This is the opposite assumption from that originally made in computing NIEL, where all displacement energy was taken to be equivalent for producing electrically active damage.

Unfortunately, the research described in [1][37] on the effects of damage clusters did not address the relationship between the physical structure of defect clusters and their electrical properties. With the techniques now available to compute the statistical properties of large numbers of structures such as that shown in Fig. 3, it is clear that such a correlation is needed.

For example, the relationship between deposited energy and the electrical activity of the resultant damage can depend on the majority carrier type, as shown in [31]. This produces an apparent difference in displacement damage in p- and n-type materials despite similar radiation exposure. Such a difference is almost impossible to imagine on the basis of collision energetics alone.

Another striking aspect of Fig. 3 is the overall size and spatial correlation of the apparent damage produced by the recoil nucleus. Simulations of this kind reinforce the notion that displacement single events may be electrically significant [38], particularly if a structure such as shown in Fig. 3 crosses an insulator or a thin sensitive volume. Might a chain of defects such as in Fig. 3 support hopping conduction and thereby short an insulator, leading to leakage or catastrophic failure? The Monte Carlo computation described here makes it possible to test such hypotheses through the statistics of $F_n(\vec{z},\vec{p};\vec{x})$ [39].

The nonionizing energy density $F(\vec{z},\vec{p};\vec{x})$ and the distribution of individual events that it represents are physically based, can be obtained for any primary particle, radiation spectrum or device geometry, and can serve as a firm starting point in a multi-step computation of electrically active defect density.

Appendix B

In this appendix, the meaning of the Lindhard partition function [26] is explored in greater detail. Norgett, Robinson and Torrens [30] have produced an approximate function giving $L(T)$ that has been adopted for NIEL computations [23]. This function was derived under the assumption that the most energetic particles, those with asymptotically large energy, were still in the velocity-proportional stopping regime. In [30] the valid range is described as $25A_1^{4/3}z_1 keV$ "and possibly much less", where A_1 and z_1 are the atomic mass and atomic number of the projectile, respectively. The Monte Carlo scheme described here simulates collisions in detail, and so makes it possible to compute $L(T)$ directly.

The results of such a computation are shown in Fig. 4 for silicon recoils in (amorphous) silicon, which should be compared with Fig. 6 of [23]. (Si was chosen over GaAs for this comparison because it is elemental.) The approximation of Norgett *et al.* is also shown in Fig. 4 for comparison [30]. The computed values match Lindhard's prediction very well for low energy primary particles. The difference is almost certainly due to the screening functions that were used, Thomas-Fermi by Lindhard, ZBL here.

At higher energies, particularly above the Bragg peak, which for silicon ions in Si is about 20 MeV, there is a notable increase of the actual value of $L(T)$ above the Lindhard-Robinson curve. Interestingly, Lindhard, *et al.*, realized this would happen and commented on it on p. 31 of [26], also showing the effect graphically in their Fig. 10 on p. 36. However, since the focus of their work was low-energy ion-solid interactions, no correction to the "partition" was attempted.

Of even greater importance than the asymptotic form of $L(T)$ is the effect on its value of the target geometry. The thickness of the target used to compute Fig. 4(a) was 10 mm (note *millimeters*). To gain an appreciation of the significance of the non-locality implicit in using the Lindhard partition, Fig. 4(a) also has curves of the computed values $L(T)$ for $10\mu m$ and $500\mu m$. The computed values fall far below the Lindhard-Robinson curve when the thickness of real samples is considered. Only in large samples away from boundaries in rigorously isotropic radiation is it completely safe to ignore this geometrical dependence. Moreover, it is apparently not well known that extending the asymptotic range of $L(T)$ to a GeV, as in Fig. 3 of [4] or Fig. 6 of [23] is inconsistent with the defining assumptions. Compare, in particular, Figs. 6 and 10 of reference [26]. $L(T)$ is only asymptotically constant for velocity-proportional stopping, and for high-energy particles the energy represented by is deposited quite far from the vertex at which it is tallied by (1). The casual reader might look at Fig. 5(a) and be tempted to conclude that one need only replace $L(T)$ in (1) by the computed partition as a correction. However, this would be misguided. The effort to compute a correction for a real system in this way would exceed that needed to compute the deposited energy density as a function of position from first principles. Fig. 4(b) presents a computation of the Lindhard partition function for protons. This curve clearly demonstrates that the Lindhard-Robinson function should never be used to estimate damage by light spallation fragments.

Acknowledgments

We thank Ron Schrimpf and Robert Reed for many helpful discussions and Emily Deaton for her cooperation at critical times during the preparation of this manuscript.

References

[1] J. Srour, C. J. Marshall, and P. W. Marshall, "Review of displacement damage effects in silicon devices," *IEEE Transactions on Nuclear Science*, vol. 50 III, no. 3, pp. 653–670, 2003.

[2] R. Reed, C. Poivey, P. Marshall, K. LaBel, C. Marshall, S. Kniffin, J. Barth, and C. Seidleck, "Assessing the impact of the space radiation environment on parametric degradation and single-event transients in optocouplers," *IEEE Transactions on Nuclear Science*, vol. 48, no. 6, pp. 2202–2209, 2001.

[3] E. A. Burke, "Energy dependence of proton-induced displacement damage in silicon," *IEEE Transactions on Nuclear Science*, vol. NS-33, no. 6, pp. 1276–1281, 1986.

[4] E. A. Burke, C. J. Dale, A. B. Campbell, G. P. Summers, W. J. Stapor, M. A. Xapsos, T. Palmer, and R. Zuleeg, "Energy dependence of proton-induced displacement damage in gallium arsenide," *IEEE Transactions on Nuclear Science*, vol. NS-34, no. 6, pp. 1220–1226, 1987.

[5] S. Agostinelli, J. Allison, K. Amako, J. Apostolakis, H. Araujo, P. Arce, M. Asai, D. Axen, S. Banerjee, G. Barrand, F. Behner, L. Bellagamba, J. Boudreau, L. Broglia, A. Brunengo, H. Burkhardt, S. Chauvie, J. Chuma, R. Chytracek, G. Cooperman, G. Cosmo, P. Degtyarenko, Dell, G. Depaola, D. Dietrich, R. Enami, A. Feliciello, C. Ferguson, H. Fesefeldt, G. Folger, F. Foppiano, A. Forti, S. Garelli, S. Giani, R. Giannitrapani, D. Gibin, J. Gomez Cadenas, I. Gonzalez, G. Gracia Abril, G. Greeniaus, W. Greiner, V. Grichine, A. Grossheim, S. Guatelli, P. Gumplinger, R. Hamatsu, K. Hashimoto, H. Hasui, A. Heikkinen, A. Howard, V. Ivanchenko, A. Johnson, F. Jones, J. Kallenbach, N. Kanaya, M. Kawabata, Y. Kawabata, and M. Kawaguti, "Geant4 - a simulation toolkit," *Nuclear Instruments and Methods in Physics Research, Section A: Accelerators, Spectrometers, Detectors and Associated Equipment*, vol. 506, no. 3, pp. 250–303, 2003.

[6] M. Mendenhall and R. Weller, "An algorithm for computing screened Coulomb scattering in Geant4," *arXiv reference arXiv:physics/0406066, Nuclear Instruments and Methods in Physics Research, Section B: Beam Interactions with Materials and Atoms*, 2004, in press.

[7] A. Barry, A. Houdayer, P. Hinrichsen, W. Letourneau, and J. Vincent, "Energy dependence of lifetime damage constants in GaAs LEDs for 1-500 MeV protons," *IEEE Transactions on Nuclear Science*, vol. 42, no. 6, pp. 2104–2107, 1995.

[8] R. Reed, P. Marshall, C. Marshall, R. Ladbury, H. Kim, L. X. Nguyen, J. Barth, and K. LaBel, "Energy dependence of proton damage in AlGaAs light-emitting diodes," *IEEE Transactions on Nuclear Science*, vol. 47, no. 6, pp. 2492–2499, 2000.

[9] S. R. Messenger, R. J. Walters, E. A. Burke, G. P. Summers, and M. A. Xapsos, "NIEL and damage correlations for high-energy protons in gallium arsenide devices," *IEEE Transactions on Nuclear Science*, vol. 48, no. 6, pp. 2121–2126, 2001.

[10] G. Summers, E. Burke, M. Xapsos, C. Dale, P. Marshall, and E. Petersen, "Displacement damage in GaAs structures," *IEEE Transactions on Nuclear Science*, vol. 35, no. 6, pp. 1221–1226, 1988.

[11] J. Biersack, "Monte Carlo and other simulation codes for ion-induced radiation effects," *Radiation Effects and Defects in Solids*, vol. 129, no. 1-2, pp. 15–17, 1994.

[12] J. F. Ziegler, "SRIM-2003," *Nuclear Instruments and Methods in Physics Research, Section B: Beam Interactions with Materials and Atoms*, vol. 219-220, no. 1-4, pp. 1027–1036, 2004.

[13] M. Mendenhall and R. Weller, "Algorithms for the rapid computation of classical cross sections for screened Coulomb collisions," *Nuclear Instruments and Methods in Physics Research, Section B: Beam Interactions with Materials and Atoms*, vol. 58, no. 1, pp. 11–17, 1991.

[14] J. Ziegler, J. P. Biersack, and U. Littmark, *The Stopping and Range of Ions in Solids*. Pergamon Press, 1985, vol. 1.

[15] J. Biersack and L. Haggmark, "A Monte Carlo computer program for the transport of energetic ions in amorphous targets," *Nuclear Instruments and Methods*, vol. 174, no. 1-2, pp. 257–269, 1980.

[16] S. R. Messenger, E. A. Burke, M. A. Xapsos, G. P. Summers, R. J. Walters, I. Jun, and T. Jordan, "NIEL for heavy ions: An analytical approach," *IEEE Transactions on Nuclear Science*, vol. 50, no. 6, pp. 1919–1923, 2003.

[17] J. Lindhard, M. Scharff, and H. Schiøtt, "Range concepts and heavy ion ranges," *Kongelige Danske Videnskabernes Selskab, Matematisk-Fysiske Meddelelser*, vol. 33, no. 14, pp. 1–42, 1963.

[18] F. Seitz and J. Koehler, *Displacement of atoms during irradiation*, Academic Press, 1956, vol. 2, pp. 305–448.

[19] C. Aguiar, A. Aleixo, and C. Bertulani, "Elastic Coulomb scattering of heavy ions at intermediate energies," *Physical Review C (Nuclear Physics)*, vol. 42, no. 5, pp. 2180–2186, 1990.

[20] C. Dale, L. Chen, P. McNulty, P. Marshall, and E. Burke, "Comparison of Monte Carlo and analytic treatments of displacement damage in Si microvolumes," *IEEE Transactions on Nuclear Science*, vol. 41, no. 6, pp. 1974–1983, 1994.

[21] M. Mendenhall and R. Weller, "An algorithm for ab initio computation of small-angle multiple scattering angular distributions," *Nuclear Instruments and Methods in Physics Research, Section B: Beam Interactions with Materials and Atoms,* vol. 93, no. 1, pp. 5–10, 1994.

[22] I. Jun, M. A. Xapsos, S. R. Messenger, E. A. Burke, R. J. Walters, G. P. Summers, and T. Jordan, "Proton nonionizing energy loss (NIEL) for device applications," *IEEE Transactions on Nuclear Science*, vol. 50, no. 6, pp. 1924–1928, 2003.

[23] I. Jun, "Effects of secondary particles on the total dose and the displacement damage in space proton environments," *IEEE Transactions on Nuclear Science*, vol. 48, no. 1, pp. 162–175, 2001.

[24] A. Akkerman, J. Barak, M. Chadwick, J. Levinson, M. Murat, and Y. Lifshitz, "Updated NIEL calculations for estimating the damage induced by particles and γ-rays in Si and GaAs," *Radiation Physics and Chemistry*, vol. 62, no. 4, pp. 301–310, 2001.

[25] I. Jun and W. McAlpine, "Displacement damage in silicon due to secondary neutrons, pions, deuterons, and alphas from proton interactions with materials," *IEEE Transactions on Nuclear Science*, vol. 48, no. 6, pp. 2034–2038, 2001.

[26] J. Lindhard, V. Nielsen, M. Scharff, and P. Thomsen, "Integral equations governing radiation effects," *Kongelige Danske Videnskabernes Selskab, Matematisk-Fysiske Meddelelser*, vol. 33, no. 10, pp. 1–42, 1963.

[27] L. Waters, "MCNPX user's manual: Version 2.1.5," Los Alamos National Laboratory, Tech. Rep., 1999.

[28] N. Bohr, "The penetration of atomic particles through matter," *Kongelige Danske Videnskabernes Selskab, Matematisk-Fysiske Meddelelser*, vol. 18, no. 8, pp. 1–144, 1948.

[29] M. P. R. Waligorski, R. N. Hamm, and R. Katz, "The radial distribution of dose around the path of a heavy ion in liquid water," *Nuclear Tracks and Radiation Measurement*, vol. 11, pp. 309–319, 1986.

[30] M. Norgett, M. Robinson, and I. Torrens, "A proposed method of calculating displacement dose rates," *Nuclear Engineering and Design*, vol. 33, no. 1, pp. 50–54, 1975.

[31] G. P. Summers, E. A. Burke, P. Shapiro, S. R. Messenger, and R. J. Walters, "Damage correlations in semiconductors exposed to gamma, electron and proton radiations," *IEEE Transactions on Nuclear Science*, vol. 40, no. 6, pp. 1372–1379, 1993.

[32] R. Reed, P. McNulty, and W. Abdel-Kader, "Implications of angle of incidence in SEU testing of modern circuits," *IEEE Transactions on Nuclear Science*, vol. 41, no. 6, pp. 2049–2054, 1994.

[33] R. A. Reed, P. W. Marshall, H. S. Kim, P. J. McNulty, B. Fodness, T. M. Jordan, R. Reedy, C. Tabbert, M. S. Liu, W. Heikkila, S. Buchner, R. Ladbury, and K. A. LaBel, "Evidence for angular effects in proton-induced single-event upsets," *IEEE Transactions on Nuclear Science*, vol. 49 I, no. 6, pp. 3038–3044, 2002.

[34] A. H. Johnston, T. Miyahira, G. M. Swift, S. M. Guertin, and L. D. Edmonds, "Angular and energy dependence of proton upset in optocouplers," *IEEE Transactions on Nuclear Science*, vol. 46, no. 6, pp. 1335–1341, 1999.

[35] K. Winterbon, P. Sigmund, and J. Sanders, "Spatial distribution of energy deposited by atomic particles in elastic collisions," *Kongelige Danske Videnskabernes Selskab, Matematisk-Fysiske Meddelelser*, vol. 37, no. 14, pp. 5–61, 1970.

[36] A. Ruzin, G. Casse, M. Glaser, A. Zanet, F. Lemeilleur, and S. Watts, "Comparison of radiation damage in silicon induced by proton and neutron irradiation," *IEEE Transactions on Nuclear Science*, vol. 46, no. 5, pp. 1310–1313, 1999.

[37] O. L. Curtis and J. R. Srour, "Recombination within disordered regions: influence of barrier height on recombination rate and injection level effects," *IEEE Transactions on Nuclear Science*, vol. NS-20, pp. 196–203, 1973.

[38] P. W. Marshall, C. J. Dale, and E. A. Burke, "Proton-induced displacement damage distributions and extremes in silicon microvolumes," *IEEE Transactions on Nuclear Science*, vol. 37, no. 6, pp. 1776–1783, 1990.

[39] R. A. Weller, A. L. Sternberg, L. W. Massengill, R. D. Schrimpf, and D. M. Fleetwood, "Evaluating average and atypical response in radiation effects simulations," *IEEE Transactions on Nuclear Science*, vol. 50, no. 6, pp. 2265–2271, 2003.

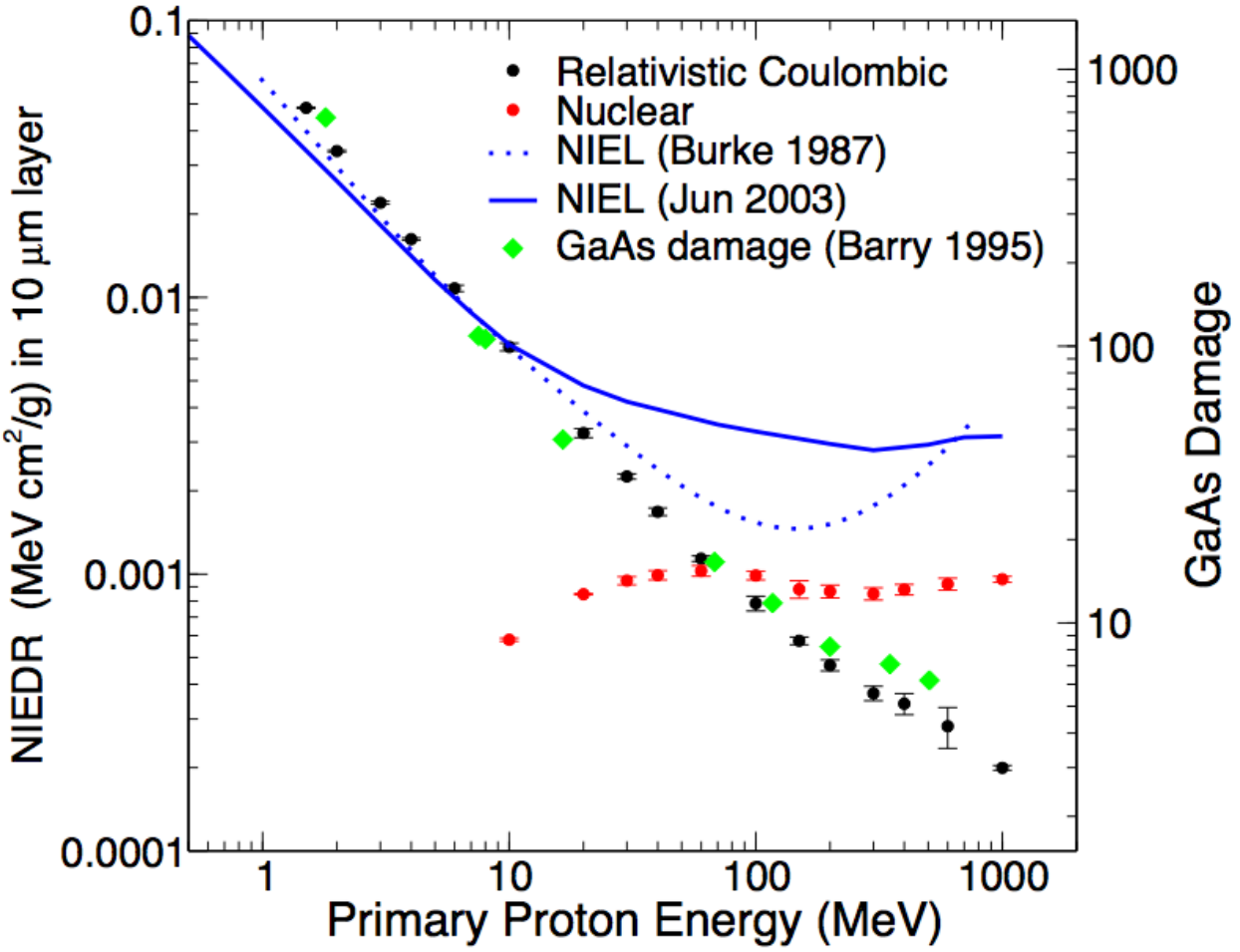

Fig. 1: The nonionizing energy deposition rate for protons in GaAs, NIEDR from equation (4), computed by the methods of this publication. Contributions from Coulombic beam-target interactions and those produced by nuclear reaction fragments, including hadronic elastic recoils, are plotted separately. NIEL from [4] and [22], and the data of Barry, *et al.*, [7] are shown for comparison. The left and right scales are adjusted to match computations and data at low energies.

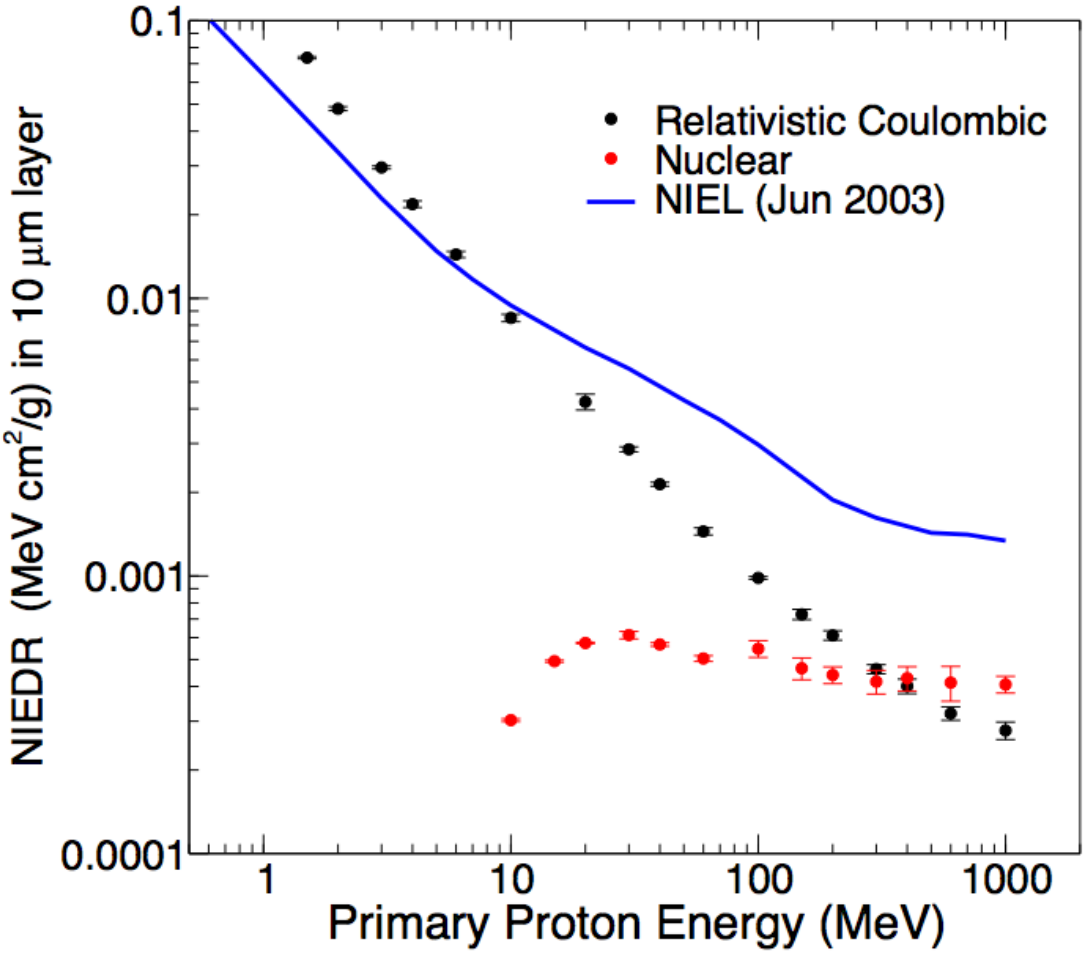

Fig. 2: The nonionizing energy deposition rate for protons in Si, NIEDR from equation (4), computed by the methods of this publication along with NIEL from [22]. Contributions to NIEDR from Coulombic beam-target interactions and those produced by nuclear reaction fragments, including hadronic elastic recoils, are plotted separately. NIEL sums these components.

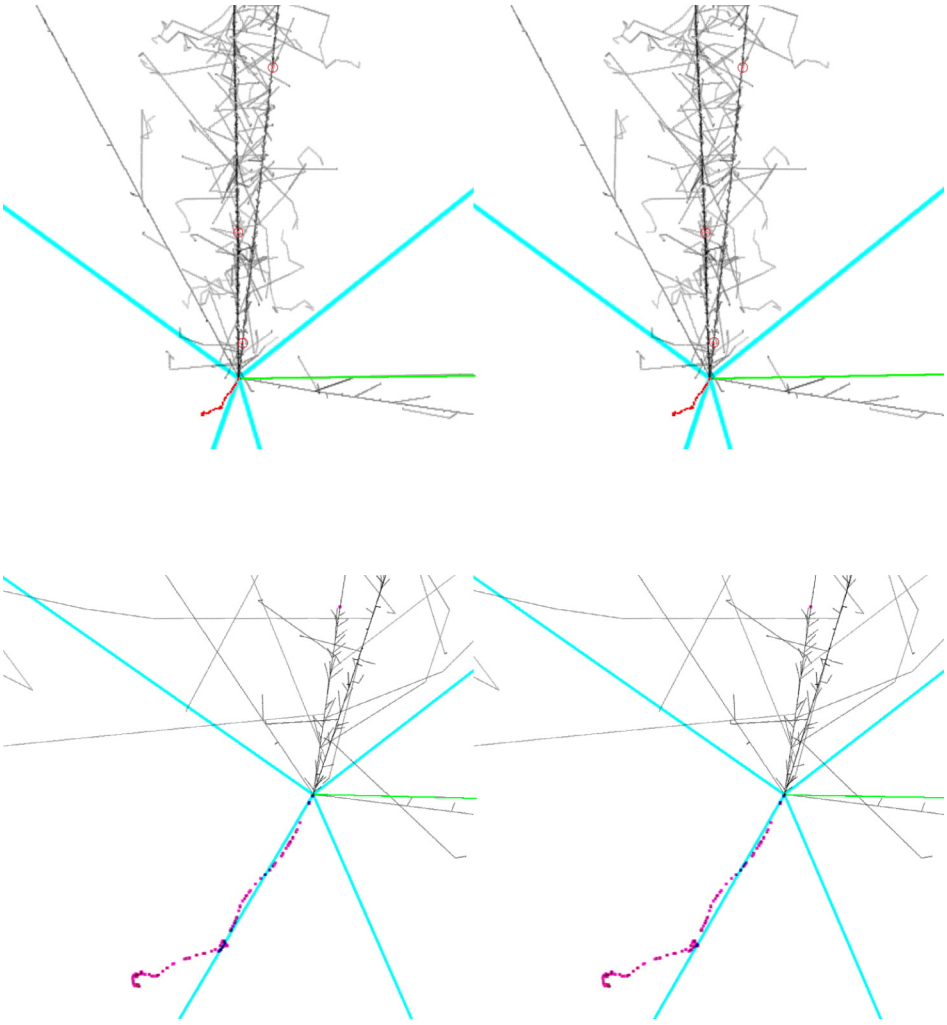

Fig. 3: A stereogram showing the ionizing (black) and nonionizing (red) energy density as a function of position for a single 100 MeV proton (green trajectory) interacting with ^{75}As in GaAs. Views 3(a) and 3(b) show the same event with different length scales. The distance between the vertex and the position at which the residual nucleus, whose trajectory is shown as a sequence of red dots, comes to rest is approximately 0.5 μm. The left and right images of each figure can be fused optically to view the event in three dimensions.

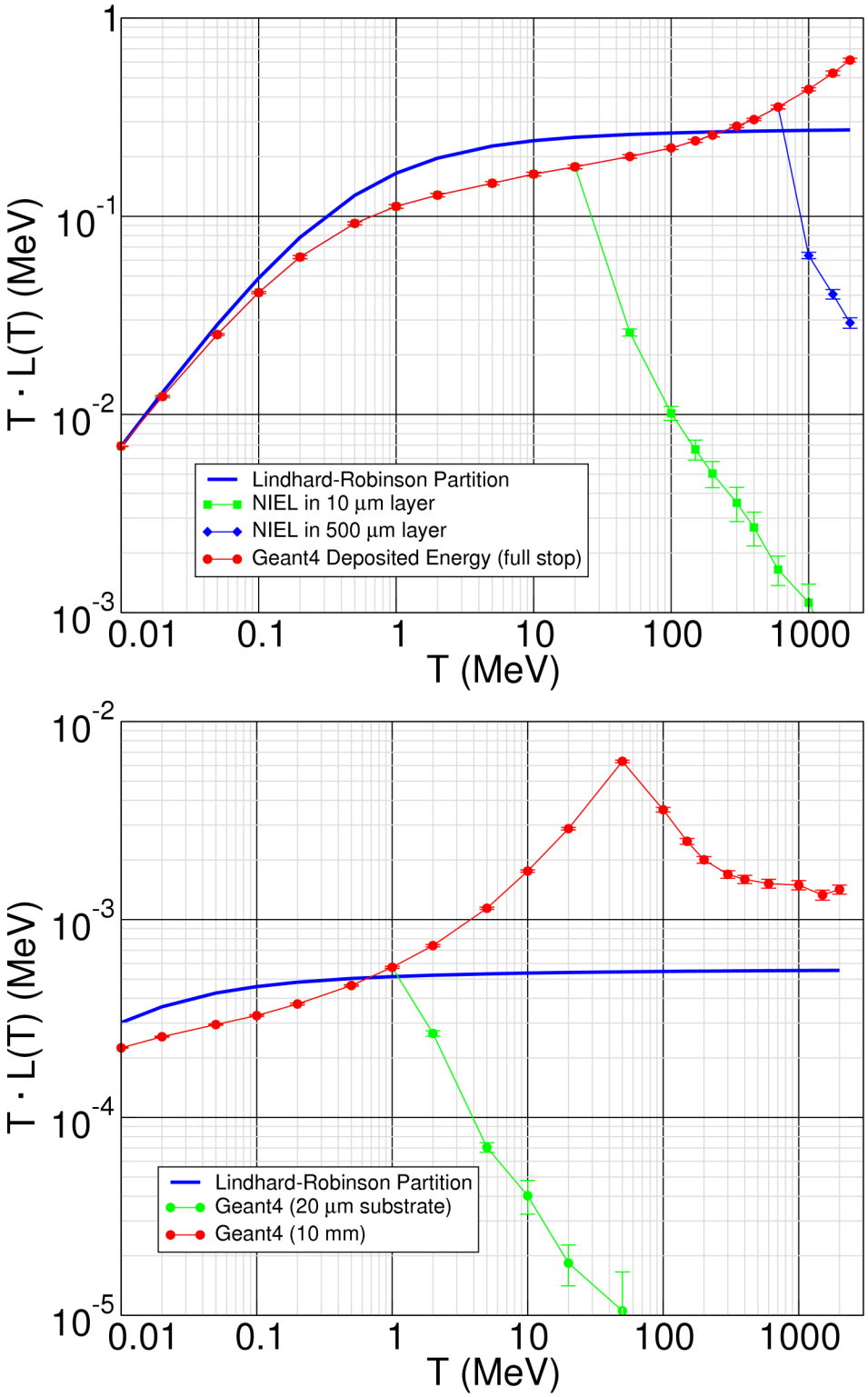

Fig. 4: Damage energy in silicon versus projectile energy for incident silicon (a) and protons (b). In each case, the solid (blue) line is the Lindhard-Robinson partition $L(T)$ given by equations (5)-(9) of [30]. The red curve in each case is the computed value of the damage energy for a full 10 mm thickness of Si. The other curves are the damage energy for thinner sections of material.